



Experimental and numerical investigation of the generated heat in polypropylene sheet joints using friction stir welding (FSW)

Reza Mirabzadeh¹ · Vali Parvaneh¹ · Amir Ehsani¹

Received: 25 December 2020 / Accepted: 9 March 2021 / Published online: 23 March 2021
© The Author(s), under exclusive licence to Springer-Verlag France SAS, part of Springer Nature 2021

Abstract

In this paper, we aim to investigate the heat generated during friction stir lap welding in polypropylene sheets. In this method, the generated heat significantly depends on the tool's rotational and linear speed, geometry, and tilt angle. Heat analysis and measurement during welding are performed numerically to validate the experimental results. A 3-D symmetric Finite Element (FE) model was created to estimate the generated and distributed heat. As is shown, the heat is mainly generated around and underside the tool due to the high friction between the rotating tool and the workpiece. This paper provided a good intuition on the generated and distributed heat during the FSW process, which can be considered a reference to produce optimum and high-quality products with fewer tests. Therefore, in this paper, the effect of a number of parameters on the generated heat during the welding process is studied experimentally and statistically and simulated in three different levels. The obtained results demonstrated a significant relationship between the properties and process parameters using analysis of variance (ANOVA) and response surface method (RSM) (Box-Behnken). Moreover, the results revealed that the effect of parameter interactions could be evaluated using the proposed mathematical model by analyzing the presented plots. In addition, the results from the simulated model using finite element software and Altair's HyperWorks confirmed the mathematical model estimations and the experimental results. The created model can successfully predict 92% of the welding joint temperature using the conditions and materials proposed in this paper. The results of the simulation analysis were validated and compared with the experimental tests, indicating a temperature difference of approximately 6%. The most effective parameter in heat generation is the rotational speed of the tool, which is responsible for up to 70% of the overall heat. Tool's geometry (15%), traveling speed (11%), and tilt angle (4%) are the other parameters effective in generating heat in the process, in respective order.

Keywords Friction-stir welding · Tensile strength · Polypropylene sheets · Optimization model · ANOVA analysis · Finite element method · Heat generation

Introduction

In recent years, the utilization of metal in transportation, construction, and aviation industries is vastly replaced by thermoplastics due to several advantages such as lighter weight, flexibility in design, low production costs, higher toughness, thermal and electrical insulation, and corrosion resistance [1]. However, plastics have several disadvantages in operation, including various primary defects such as limited operating

temperature and low strength. To overcome these problems and provide geometrical and dimensional immutability, plastic materials are produced in integrated forms and are jointed permanently, rather than semi-permanent or temporary.

Several methods are employed to join polymers, including adhesive joint, mechanical joint, and fusion welding [2]. Among these methods, the FSW is currently prevalent in polymer joining since it does not require filler materials and external energy sources, provides homogeneity in the welding zone and minimum heat shocks on the workpiece, does not alter the physical and chemical properties of the based material, and offers desirable mechanical properties [3]. The FSW method is a novel technique invented at The Welding Institute (TWI) in 1991. It is considered an environmental-friendly process (due to the lack of filler material) and is known as a solid-state bonding process. Moreover, it prevents large distortions,

✉ Vali Parvaneh
vali.parvaneh@gmail.com; vali.parvaneh@iau-shahrood.ac.ir

¹ Department of Mechanical Engineering, Shahrood branch, Islamic Azad University, Shahrood, Iran

cracks caused by thermal shocks, the formation of large dendritic structures, the occurrence of porosity and shrinkage, oxidation and discoloration, and creates an effective area of vast heat at the junction. In addition, it prevents the formation of fragile areas between the heterosexual material and high energy consumption. In this method, the heat required at the joint relies on the thermal energy generated by the mechanical friction between the rotating tool and the workpiece [4, 5]. This paper investigates the heat generated in the pin region during the FSW process, with a specific concentration on the heat generated under the pin and its side. The friction between the workpiece and tool will generate frictional heat. This heat will degrade the strength of the polymer pieces prior to reaching the melting point, which moves the tool along the weld path, resulting in the solid-state joining of the two pieces.

Solid-state welding provides an excellent opportunity to increase commercial application of polymers. Recently, FSW is used in commercial polymer joining, including the formation of strong bonds in the turbulent region and the region under the influence of thermomechanical force (due to macromolecular agitation) and the joining of stirred carbon fiber in the bond using thermomechanical behavior for the carbon-fiber-reinforced polyetherimide in the point friction welding process [6]. Moreover, commercial applications of this welding method include constructing jets and nuclear waste storage tanks and connecting heterosexual materials in car hulls, decks of warship structures, parts in shape, non-linear geometries, and the floor panels of the trains [7].

As shown in the research on polymers, it is better to use FSW in polymer joining to achieve a high-strength structure. The reason is that in this method, the workpiece remains solid, and its properties are not degraded [8]. However, existing problems and challenges, including the reliability and structural integrity of the welding, necessitated advancement in FSW technology. Therefore, novel control strategies have been developed on the following three inherent issues: (1) supporting the back and fixing the root penetration problem by designing the bobbin tool FSW in the FSW process (BT-FSW), self-support FSW (SSFSW), and penetrating FSW (PFSW), (2) removing weld thinning in FSW using the stationary shoulder FSW (SSFSW2) and the micro-plunge-depth FSW (MPD-FSW), and (3) eliminating keyholes and other defects of the FSW process (regenerative processes) such as friction plug welding (FPW), and filling friction stir welding (FFSW) [9].

As indicated in [10–13], the tool's geometry, rotational and traveling speed, and tilt angle are the effective parameters on the welding quality, among which the cylindrical-conical pin offers the most effective geometry. They found that enhancing the rotational speed and reducing the traveling speed of the tool yields more heat and influences the welding properties. Moreover, the effect of pin angle on the surface quality is also investigated in these studies. In specific, they observed that an

effective tool angle leads to more plunging and better material mixing, while higher rotational speed and tool angle fails to produce the desired outcome [14]. Adopting an optimum tool tilt angle, employing stationary shoulder, and preheating have been recommended to control the welding process and provide a successful FSW [10, 15].

Similar results were reported for different pin geometries (square, triangular, threaded, and conical) for a vast range of rotational and traveling speeds [16]. An appropriate selection of effective parameters on the produced pieces (using FSW) is essential. In other words, if a high rotational speed is selected during PE welding, the exorbitance heat is generated, and consequently, melted material may outpour from the welding line border [10, 17]. Moreover, researchers carried out several studies on the analytical modeling of FSW. Based on their experimental evaluations, a model was obtained for the calculation and analysis of friction factor in FSW [18].

The thermo-mechanical model simulation of FSW is another issue investigated in the literature. In specific, [19] reported that the flow of material closer to the surface of the workpiece depends on the rotational speed of the shoulder. Thermo-mechanical analysis of the FSW using the FE method was performed in [20]. In this study, the researchers presented a thermal model to demonstrate temperature history in accordance with the experimental data. Moreover, The FE method was employed in [21] to model the FSW temperature, and an FE model was developed according to this method for the evaluation of temperature distribution in plates welded using the FSW process.

The processing parameters were also studied based on both thermal and mechanical outputs of Friction Stir Welded 2024-T3 Aluminum alloy. In [22], they predicted the thermal behavior and residual stress of the alloy using the ANSYS software. Arif et al. used FEM to obtain the maximum temperature during friction stir welding of aluminum alloy and validated the numerical results through comparison with the corresponding experimental outcomes [23]. Using the numerical method, the researchers presented a numerical evaluation model to accurately and practically analyze the FSW results. Moreover, they introduced the threaded tool as an effective structure in material agitation. However, this structure has a high risk of failure during FSW operations. The most optimal model reported with threaded cone pin has 800RPM rotational speed and 30 mm/min linear speed [24].

In [25], the HyperWorks software was employed to study the temperature distribution in FSW based on FEM. As demonstrated there, during FSW, under and around the shoulder are the heat-affected zones. Another research investigated the temperature distribution during FSW using ANSYS and HyperWorks [26]. The effect of transverse tool speed on FSW is investigated numerically by Zhao Zhang and Hong Wu Zhang using a thermo-mechanical model. As demonstrated in that study, when the transverse speed is increased, the

stirring effect of the welding tool weakens, which is the reason for the weld flaw [27].

The FE modeling is employed in [28] to determine the maximum temperature in FSW. In this study, the numerical results were validated, and the maximum temperature in the FSW for stainless steel was studied using ANSYS. Moreover, the researchers conducted a comprehensive study of heat transfer in polymer foams using the Response Surface Method (RSM). In this study, a regression model was provided to predict the overall thermal conductivity using variance analysis with a maximum error of 4% [29]. Using the analysis of variance (ANOVA) and Taguchi theory, Azdest et al. optimized the impact resistance of the polymer-based nanocomposites by optimizing the rotational and linear velocity of the tool in the FSW process [30]. In addition, they successfully optimized the tensile strength of the high-density polyethylene friction welded pipes with similar performance, indicating that the rotational speed is the most effective parameter for increasing the tensile strength of the welded pipes [31]. Furthermore, the effect of parameter interactions on the shrinkage of polycarbonate in the injection molding process was studied in [32]. They proposed a regression model to estimate the shrinkage rate. Finally, Hassanzadeh et al. employed ANOVA to predict the thermal conductivity of polymer foams and obtained significant relationships between the effects of foam density and cell size on various thermal conduction mechanisms [33].

The RSM method was proposed by Mendes et al. to model and optimize FSW in polymers [34]. Azarsa et al. employed RSM as a statistical method to estimate mechanical properties. They proposed a meaningful relationship between mechanical properties and welding parameters of high-density polypropylene plates [35]. Rahbarpor et al. [36] and Mostafapour et al. [37] studied the feasibility and welding quality of plastic composites, along with the effect of input parameters on the tensile strength of the joint. In specific, they analyzed the jointed workpieces using RSM and concluded that the generated heat is significantly effective on the maximum tensile strength. Moreover, Bagheri et al. studied the mechanical characteristics of acrylonitrile butadiene styrene (ABS) sheets

welded using FSW and proposed a significant relationship between the mechanical properties of workpiece and processing parameters using ANOVA and RSM [38].

In the present paper, DOE (Design of Experiment) software and RSM were employed to investigate the effects of various parameters on the heat generated during FSW in three different levels. In specific, three rotational tool speeds (1000–850–700 rpm), travel tool speeds (70–50–30 mm/min), tilt angles (0–1–2 degree), and shoulder to pin diameter ratios (12.4–12.5–12.6) are the effective parameters. The range of the input parameters has been selected according to previous studies and through preliminary experimental verifications. Moreover, axial force, workpiece restraint force, ambient temperature, and the material employed for tool and workpiece are considered the fixed parameters. The obtained numerical results have been compared with the corresponding experimental results. Then, the results were analyzed using Design Expert 11 software, and a mathematical model is obtained based on effective parameters and the heat generated in the welding process.

Materials and methods

Sample preparation and method

In this paper, the sheets employed for friction stir welding were $100 \times 80 \times 6$ mm compression-molded polypropylene (Jahan Teflon Co., Iran). Samples were cut in rectangular shapes with dimensions of 80×100 mm using Guillotine. Then, two edge to edge sheets were used for welding (Fig. 1).

Hot-work steel (H13) is the most common tool for friction stir welding [39]. Therefore, a tool was prepared using 20 mm hot-work steel with the desired geometry (Fig. 2). As the studies on the tool indicate, the concave shoulder creates joints with higher strength, due to the increased thickness of the top sheet [40]. Thus, the tool shoulder was created in a concave shape with an angle of 4 degrees. Table 1 presents the specifications of the tool employed in this research. Following

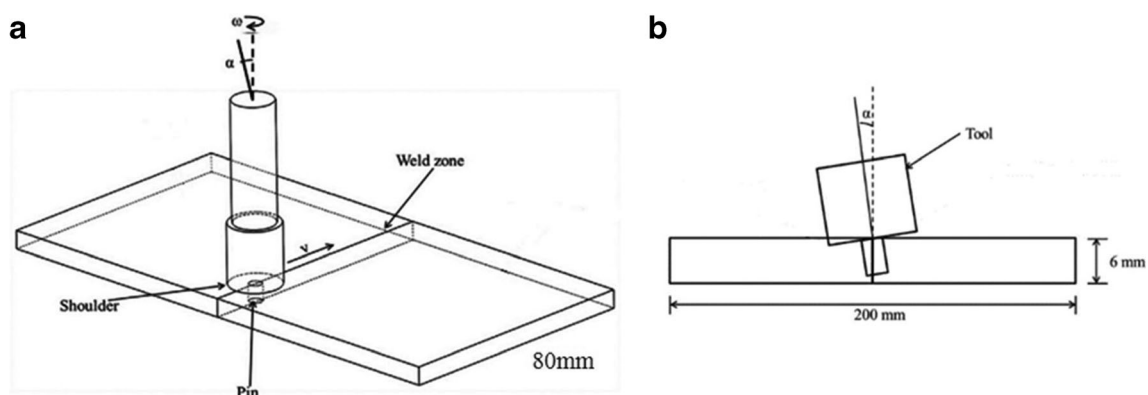


Fig. 1 A schematic of the polypropylene sample under friction-stir welding



Fig. 2 The tools employed in the study

the thermal operation, the tool was hardened to 50 HRC. Then, a special fixture was designed using a CNC milling machine to stabilize the components for the friction-stir welding. Accordingly, polypropylene sheets with dimensions of 80×200 mm were constructed. Figure 3 illustrates an image of the fixture.

The proper selection of process parameters is vital in achieving a proper joint and an excellent tensile strength. For this purpose, it is important to understand the properties of the material to examine the effect of production parameters on the tensile strength of the joints. Table 2 provides the properties of the polypropylene employed in this study at 25 °C.

Calculating the generated heat

A thermal camera (CA 1950 DiaCAM 2 thermal camera, Chauvin Arnoux, United Kingdom) with a calculation range of -20 to $+250$ °C is used to evaluate the generated heat. The temperature of the samples was measured at room temperature. To increase the reliability of temperature measurements, the experiment was repeated three times, and the average of the highest heat was recorded.

Experiment design

In the present study, RSM and Design Expert 11 were used for statistical modeling. The Box-Behnken Design (BBD), as one of the prominent types of RSM, is a quadratic design method based on three-level incomplete factorial designs [41]. This method enables parameter estimation in a quadratic model,

design measurement, and calculation of the mismatch parameter values [42].

Comparing BBD and other response surface designs (e.g., central composite or full factorial design) confirms that the efficiency of BBD is superior to both design methods. A large number of researchers have employed traditional experimental methods to evaluate the efficiency and effect of parameters in the friction-stir spot welding process [42]. To this aim, one parameter is considered a variable, while the rest are assumed constant. However, this method significantly increases the cost and time.

In the design proposed in this article, the answers were modeled by fitting a second-order polynomial expressed as Eq. (1):

$$Y = \beta_0 + \beta_1x_1 + \beta_2x_2 + \beta_3x_3 + \beta_{12}x_1x_2 + \beta_{13}x_1x_3 + \beta_{23}x_2x_3 + \beta_{11}x_1^2 + \beta_{22}x_2^2 + \beta_{33}x_3^2 \quad (1)$$

where x_1 , x_2 , and x_3 represent independent variables, β_0 shows the y-intercept, β_1 to β_{33} are fitting constants, and Y is the response (R% or q). The number of test points can be obtained from Eq. (2) [43]:

$$N = 2K(K-1) + C_0 \quad (2)$$

In this equation, K demonstrates the number of variables, and C_0 represents the number of focal points. In this paper, K and C_0 are considered 4 and 5, respectively, requiring 29 experiments. The RSM is a set of useful mathematical and statistical techniques to analyze problems and optimize the response using several independent variables that affect either a dependent variable or the response. In addition, ANOVA was used to examine the significance of the parameters. Table 3 shows the process parameters used in this study.

Results and discussion

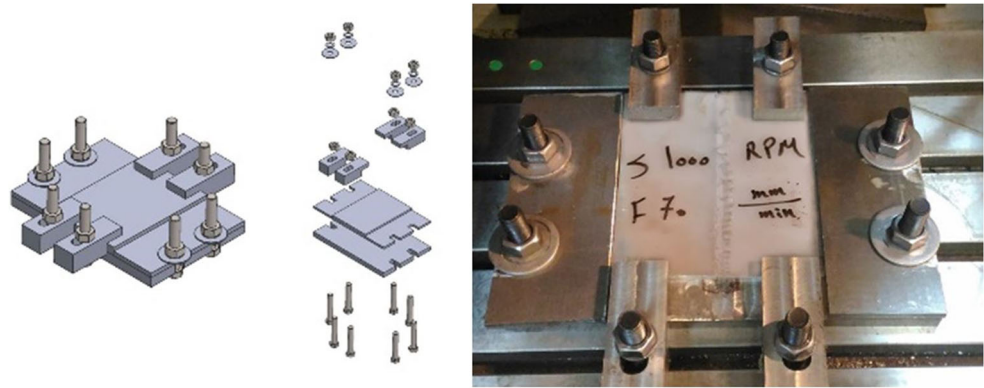
Optimization based on Box-Behnken design

The BBD was employed to evaluate the effect of the tool's rotational and travel speeds, diameter ratio, and tilt angle on the generated heat. First, the mathematical model is constructed using the BBD to define the interaction and relationships of the parameters to estimate and control the generated heat. Then, ANOVA is employed to express the effect of each parameter on the generated heat.

Table 1 Specifications of the tool used in this study

Shoulder diameter(mm)	Shoulder length (mm)	Pin profile	Pin diameter (mm)	Pin length (mm)	Shank diameter (mm)
12	15	Cylindrical	4–5–6	5.7	20

Fig. 3 The fixture used for friction-stir welding



Model creation and variance analysis

The generated heat obtained from the experimental analysis is presented in Table 4. The presented 2-D model was employed to find the relationship between input parameters and the generated heat. The regression model of the processing parameters, obtained using RSM for the response developing process, is presented in Eq. (3).

$$\begin{aligned}
 \text{Temperature} = & +31.13753 - 223.23337 D/d \\
 & + 0.711649 \text{ Rotational speed} \\
 & + 0.884917 \text{ Travel speed} \\
 & + 46.19292 \text{ Tilt angle} - 0.044933 \\
 & \quad D/d * \text{Rotational speed} - 10.74500 D/d * \\
 & \quad \text{Tilt angle} - 0.000897 \text{ Rotational speed} * \\
 & \quad \text{Travel speed} - 0.338875 \text{ Travel speed} * \\
 & \quad \text{Tilt angle} \\
 & + 55.96534 D/d^2 - 0.000289 \text{ Rotational speed}^2
 \end{aligned}
 \tag{3}$$

The results of ANOVA for the considered model are presented in Table 5. In ANOVA, R^2 is defined as the ratio of the variation of a specific parameter to the total variation. In [44], R^2 is recommended to be 0.8 to provide an appropriate estimation of the model. In this paper, R^2 and the corrected R^2 are

0.9733 and 0.9585, respectively (See Table 6), to confirm the model reaction. Moreover, the obtained values for P and F in the model were 65.61 and 0.0001, respectively, indicating the effectiveness of the created model. While a P value of less than 0.1 indicates the effectiveness of a model, higher values show ineffectiveness [44]. F-test is employed to determine the significance of the regression coefficients using the standard P value. Generally, a higher F value, as well as a lower P value, shows a higher significance level for the coefficients [45].

Statistical evaluation of the model accuracy

It is essential to evaluate the accuracy of the model to achieve an appropriate design. As can be seen in Table 6, the estimated R^2 is 0.9214, which shows a 92% predictability of the created model for a variety of outputs. Figure 4 shows normalized residuals and error percentage following the initial model correction. Moreover, it is evident in Fig. 4 that proximity to the line points indicates the absence of an outlier. In other words, data points farther from the line have a higher error percentage.

Figure 5 shows the conformity of the obtained results with the statistical model and the real values. As can be seen, there is a good agreement between the estimated results and their corresponding real values.

The effect of the four variables on the generated heat is shown in Figs. (6 and 7). In these figures, the surface response is plotted as a function of one parameter and two parameters in Figs. 6 and 7, respectively. As can be seen in Fig. 6, according

Table 2 Polypropylene properties

Melt flow index	3
Tensile strength (MPa)	34
Elongation at break (%)	350
Flexural modulus (MPa)	1310
Brittleness temp (°c)	15
Vicat softening point (°c)	154–150
Rockwell hardness (R-scale)	95
Impact strength (ft lb)	10

Table 3 The maximum and minimum level for the evaluated factors

Parameters	Units	Minimum level	Maximum level
D/d	mm/mm	2	3
Rotational speed	rpm	700	1000
Travel speed	mm/min	30	70
Tilt angle	Deg	0	2

Table 4 DOE using Box-Behnken Design, and the temperature for each experiment

Run	Factor 1 A:D/d	Factor 2 B:Rotational speed	Factor 3 C:Travel speed	Factor 4 D:Title angle	Temperature (experimental)	Predicted value	Percentage difference
	mm/mm	rpm	mm/min	Deg	°c	°c	%
1	3	850	30	1	158.64	154.36	-2.8
2	2	850	50	2	150.56	150.14	-0.3
3	2.5	850	70	2	125.67	123.51	-1.7
4	2	850	70	1	138.97	138.06	-0.7
5	2.5	1000	30	1	143.65	142.30	-0.9
6	2.5	850	50	1	131.66	132.22	0.4
7	3	850	50	2	144.68	147.05	1.6
8	3	700	50	1	135.61	137.35	1.3
9	2.5	850	50	1	132.69	132.22	-0.4
10	2.5	850	30	2	146.16	145.71	-0.3
11	2.5	850	70	0	129.63	132.29	6.5
12	3	1000	50	1	149.08	149.74	0.4
13	2	700	50	1	121.86	122.96	0.9
14	2	850	30	1	144.68	146.71	1.4
15	2.5	700	50	0	115.51	113.78	-1.5
16	2	850	50	0	136.44	134.63	-1.3
17	2.5	1000	70	1	127.85	128.28	0.3
18	2.5	700	30	1	119.36	117.80	-1.3
19	2.5	1000	50	0	135.21	132.90	-1.7
20	3	850	70	1	147.19	145.72	-1.0
21	2.5	1000	50	2	135.12	137.68	1.9
22	2	1000	50	1	148.81	148.82	0.0
23	2.5	700	50	2	118.30	118.55	0.2
24	2.5	850	30	0	123.01	127.38	3.4
25	2.5	850	50	1	135.13	132.22	-2.2
26	2.5	850	50	1	132.39	132.22	-0.1
27	2.5	700	70	1	114.32	114.53	0.2
28	3	850	50	0	152.05	153.03	0.6
29	2.5	850	50	1	130.14	132.22	1.6

Table 5 The Effect of each variable on elongation according to the variance analysis

Source	Sum of squares	df	Mean square	F-value	p value	
Model	3788.76	10	378.88	65.61	<0.0001	Significant
A-D/d	175.80	1	175.80	30.44	<0.0001	
B-Rotational speed	1097.51	1	1097.51	190.07	<0.0001	
C-Travel speed	224.21	1	224.21	38.83	<0.0001	
D-Title angle	68.35	1	68.35	11.84	0.0029	
AB	45.43	1	45.43	7.87	0.0117	
AD	115.46	1	115.46	19.99	0.0003	
BC	28.94	1	28.94	5.01	0.0380	
CD	183.74	1	183.74	31.82	<0.0001	
A ²	1351.19	1	1351.19	234.00	<0.0001	
B ²	291.13	1	291.13	50.42	<0.0001	
Residual	103.94	18	5.77			
Lack of fit	90.75	14	6.48	1.97	0.2697	Not significant
Pure error	13.19	4	3.30			
Cor total	3892.70	28				
Source	Sum of squares	df	Mean square	F-value	p value	
Model	3788.76	10	378.88	65.61	<0.0001	Significant
A-D/d	175.80	1	175.80	30.44	<0.0001	
B-Rotational speed	1097.51	1	1097.51	190.07	<0.0001	

Table 6 ANOVA results for the generated heat in the FSW process

Standard deviation	2.40	R ²	0.9733
Mean	135.32	Adjusted R ²	0.9585
C.V. %	1.78	Predicted R ²	0.9214
		Adeq precision	27.4239

to the *F* and *P* values, all the linear parameters, interactions, and quadratic parameters are effective except for *C*² and *D*². As demonstrated in Fig. 6a, when the ratio of the shoulder diameter to pin is increased, the generated heat experienced a slow increase, followed by a significant increase. Moreover, according to Fig. 6b, enhancing the rotational speed to 900 rpm increases the response surface, while such effect is not present in further enhancements. However, based on the presented plot in Fig. 6c, when the travel speed increases, the surface response declines. In other words, the travel speed has an inverse effect on the surface response. Finally, as shown in Fig. 6d, the surface response increased gradually with tool angle enhancement.

Contour plots and optimum point determination

The parameter correlations and interactions of the input parameters are presented in Fig. 7. Each plot demonstrates the effect of two variables in the selected range. It should be noted that in these plots, two parameters are considered variables, and one is constant. These plots provided a better insight into the effect of each variable on the generated heat. Contour (a)

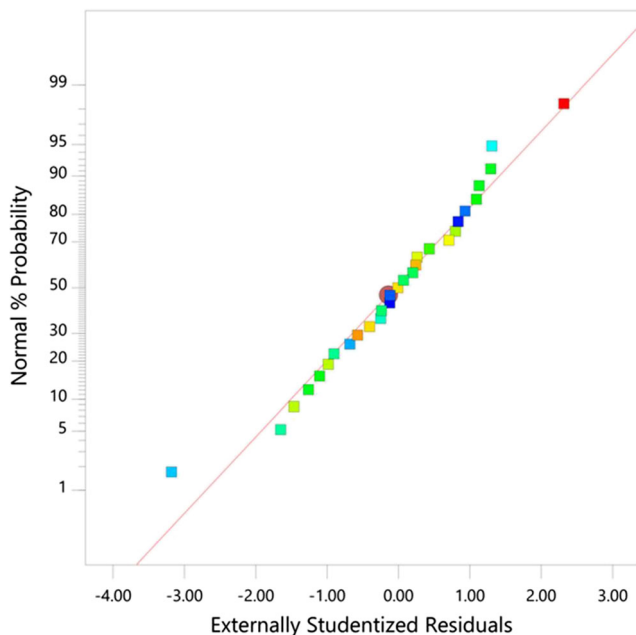


Fig. 4 Normal plot of the residuals

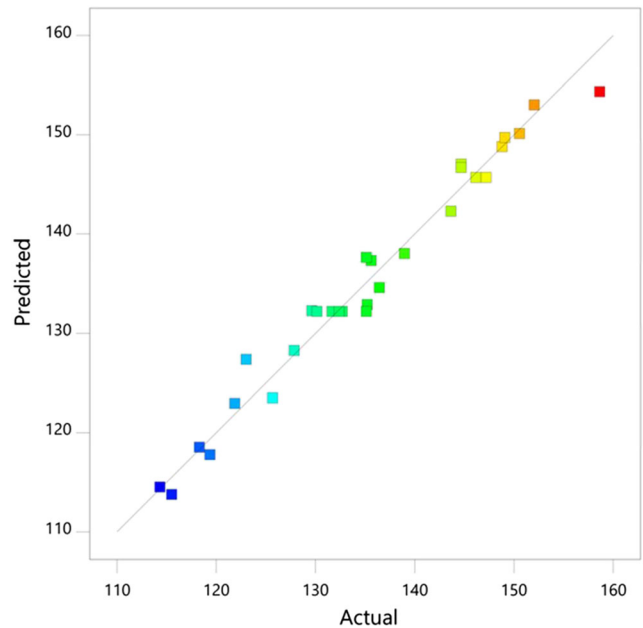


Fig. 5 Conformity of the predicted results with the actual values

demonstrates that an increase in rotational speed and the tool diameter ratio leads to a significant increase in the generated heat. On the other hand, this increment is insignificant in the case of increasing the ratio of shoulder to pin diameter. As can be seen in contour (d), the generated heat is declined by travel speed increment. Moreover, the tool angle enhancement leads to an insignificant increase in the generated heat.

Figure 8 presents an overview of the effect of all parameters on the generated heat. The results show that the tool’s rotational speed (70%), shoulder to pin diameter ratio (15%), travel speed (11%), and tilt angle (4%) affected the generated heat in the FSW process. Figure 9 illustrates the percentage of the effectiveness of each parameter.

The previous sections studied the effect of several parameters on the generated heat. Moreover, a mathematical model was created to estimate this effectiveness. The following sections aim to validate these results using numerical simulation and obtain an optimum processing temperature during FSW.

Numerical simulation of FSW

Determining the generated heat during FSW

In this section, the model is simulated numerically based on the thermo-mechanical procedure. For this purpose, first, the generated heat caused by the friction between the tool and workpiece during FSW must be calculated. During this process, heat is generated near the tool and workpiece. A simplified model of the tool is presented as follows, which can be employed to determine the generated heat. In this equation, *R*_{shoulder} is shoulder diameter, *R*_{probe} is pin diameter, and *H*_{probe} is pin height.

Fig. 6 The match percentage of statistically predicted results and actual results

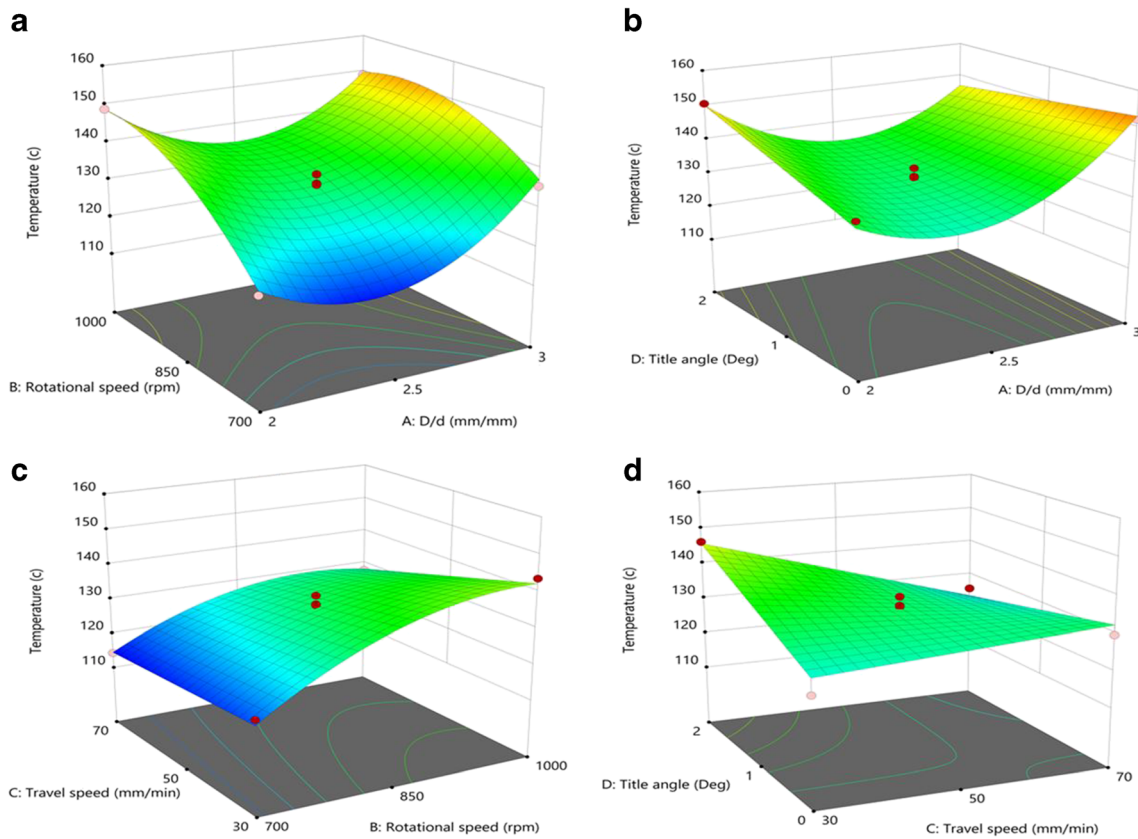
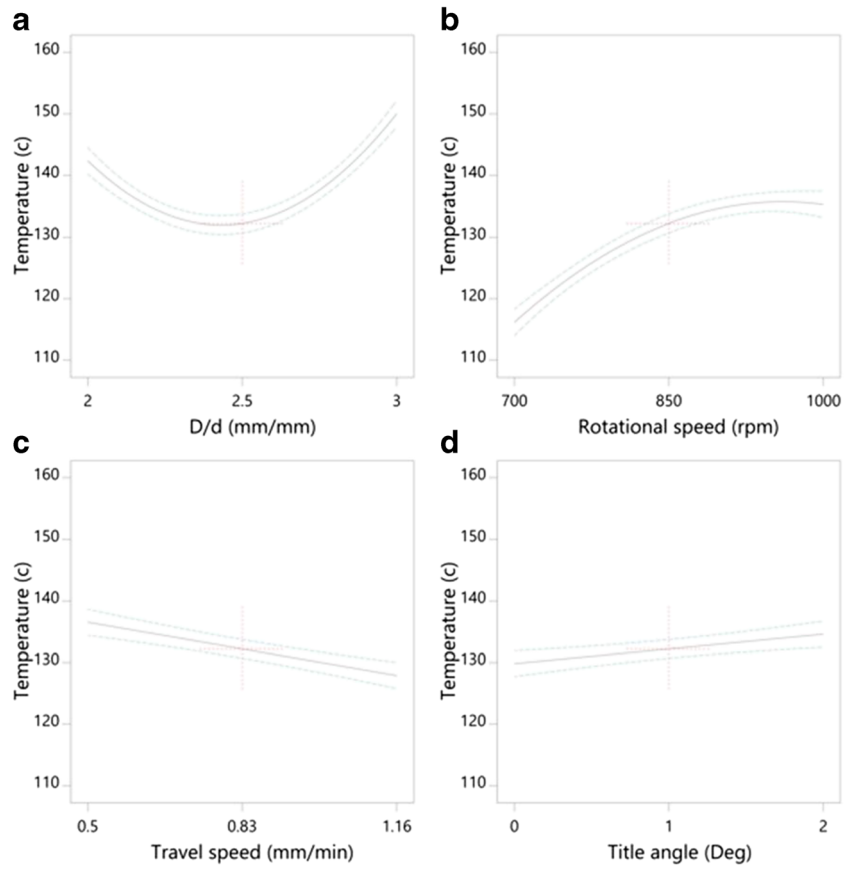


Fig. 7 Interaction of input parameters

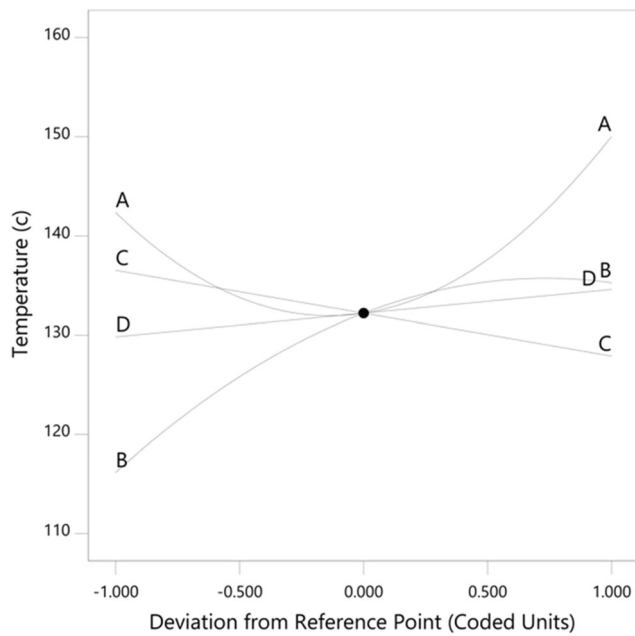


Fig. 8 The effect of the effective parameters (A: D/d, B: Rotational speed, C: Travel speed, D: Title angle) on the temperatures of the joint

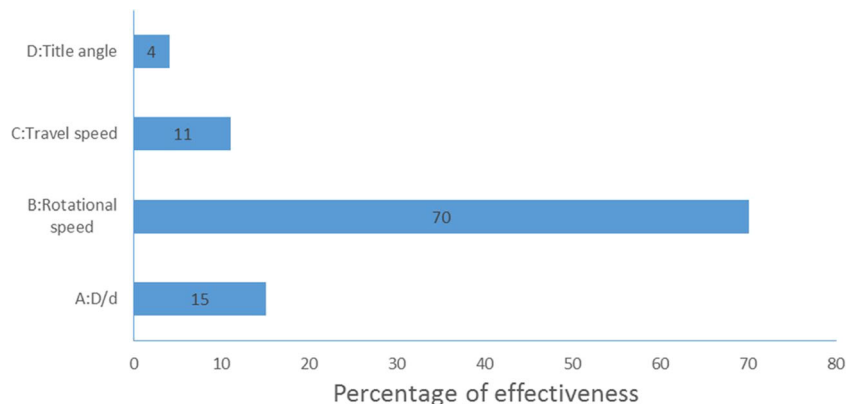
Moreover, Q_1 , Q_2 , and Q_3 are the generated heat in the shoulder, the lateral surface of the pin, and underside the pin, respectively. Thus, the overall generated heat is $Q_{total} = Q_1 + Q_2 + Q_3$. The generated heat in each contact region is determined based on Eq. (4).

$$dQ = \omega dM = \omega r df = \omega r \tau_{contact} dA \tag{4}$$

In this equation, ω is the rotational speed of the tool, M is the moment, F is force, A is the contact area, and r is the radial distance from the pin axis in the cylindrical coordinates system. Based on Eq. (4), the generated heat in the tool shoulder (Q_1) can be determined using Eq. (5).

$$Q_1 = \int_0^{2\pi} \int_{R_{probe}}^{R_{shoulder}} \omega \tau_{contact} r^2 (1 + \tan \alpha) dr d\theta = \frac{3}{2} \pi \omega \tau_{contact} (R_{shoulder}^3 - R_{probe}^3) (1 + \tan \alpha) \tag{5}$$

Fig. 9 Percentage of the effectiveness of processing parameters on the generated heat in the FSW process



The generated heat in the pin is divided into two portions: Q_2 (from the lateral surface) and Q_3 (from the underside surface). By integrating Eq. (3) in the lateral surface, the generated heat at the lateral surface is calculated based on Eq. (6).

$$Q_2 = \int_0^{2\pi} \int_0^{H_{probe}} \omega \tau_{contact} R_{probe}^2 dz d\theta = 2\pi \omega \tau_{contact} R_{probe}^2 H_{probe} \tag{6}$$

Equation (7) presents the generated heat underside the pin, obtained by integrating Eq. (3) in the pin tip.

$$Q_3 = \int_0^{2\pi} \int_0^{R_{probe}} \omega \tau_{contact} r^2 dr d\theta = \frac{2}{3} \pi \omega \tau_{contact} R_{probe}^3 \tag{7}$$

Thus, the total generated heat is determined using Eq. (8) [46].

$$Q_{total} = Q_1 + Q_2 + Q_3 = \frac{2}{3} \pi \omega \tau_{contact} \left((R_{shoulder}^3 - R_{probe}^3) (1 + \tan \alpha) + R_{probe}^3 + 3R_{probe}^2 H_{probe} \right) \tag{8}$$

Thermal simulation of FSW

Numerical simulations were performed using Altair HyperWorks 2019 according to the thermo-mechanical procedure. A $100 \times 80 \times 6$ mm plate with hexagonal elements was constructed for welding. Due to the large displacements in the friction welding process, a method must be adopted that accurately predicts heat generation and plastic strain. For this purpose, three Lagrangian, Eulerian, and coupled Lagrangian-Eulerian approaches can be used. If the Lagrangian approach is employed, there will be a deviation and excessive distortion of the elements due to the deformation and the movement of the element nodes in the translational three degrees of freedom. This distorts the elements and, ultimately, results in an inefficient analysis unless a much smaller mesh is applied to the entire model. Nevertheless, this

will increase the cost and analysis time. The Eulerian technique uses a method in which the nodes of the elements can move, while the shape of the elements is almost preserved during the plastic displacement and changes only in terms of dimensional scale.

In this paper, the coupled Lagrangian-Eulerian technique is used in the simulation. Unlike the Lagrangian element, the Eulerian elements do not change in geometry during the simulation and remain constant. The Eulerian element is initially empty, and matter must be attributed to this empty element in the desired volume. Due to the absence of distortion in Eulerian elements, they can properly model large deformations. Plus, simulations are highly cost-efficient. Dimensions and parametric conditions of the friction stir welding process were simulated by Wu et al. using the Lagrangian-Eulerian technique based on experimental working conditions [47]. In this investigation, the friction welding process pp. was simulated based on coupled Euler-Lagrange method CEL. The model (tool and workpiece) was simulated in three dimensions using the Eulerian-Lagrangian method. In addition, the Johnson-Cook model and thermal properties were used for workpiece material pp. CEL method provides the benefits of Lagrangian and Eulerian meshing methods simultaneously and can precisely simulate the physical boundary.

Using the Eulerian-Lagrangian approach, Nandan et al. numerically simulated the two processes of friction stir welding and point friction stir welding and calculated the temperature and force on the tool for both processes. Based on their results, the Lagrangian coupling Euler approach can properly predict the temperature and force required to perform welding [48]. Ansari et al. developed a three-dimension finite element model based on the coupled Eulerian-Lagrangian approach to model the heat in tools and workpiece in FSW. Based on their results, coupled Lagrangian-Eulerian technique could provide a relatively good prediction of the temperature distribution in

the tool and workpiece, along with the flow of materials in different welding areas [49]. Moreover, Eskandari et al. investigated and simulated the friction stir process of aluminum alloy using the coupled Lagrangian-Eulerian technique. Their results confirmed that this numerical method has the ability to properly analyze the stress and heat in the process [50]. The simulated model in that study possesses real-world model conditions and dimensions, and the finite element model has been developed with 2200 hexahedral elements and 2507 active nodes to simulate turbulent friction welding.

The analytical results in the present study were compared with the corresponding experimental outcomes, and accordingly, the observed temperature difference was approximately 6%. Therefore, it can be concluded that the presented model can properly estimate the temperature distribution. Based on the obtained results, the temperature distribution in the workpiece was such that even though the maximum temperature during the welding process was (158.32 °C) was enough for workpiece stirring, the material did not melt.

In this study, three successive thermal steps were considered: (1) tool rotating and plunging, (2) rotating and stirring, and (3) rotating along with travel speed. The majority of the heat was generated when the tool penetrated the polypropylene sheet. Evaluation of this heat is the primary goal of this study. Based on Eulerian mesh, the mesh shape was unchanged during analysis, while the material point was displaced in each element. The following figures represent this simulation process and its results. Figure 10 represents the definition of the tool and workpiece geometry, tool tilt angle, rotational speed, translation speed, and process parameters coupling.

Figure 11 shows the temperature distribution schematic during the FSW process. As this figure demonstrates, the red region (around and underside the shoulder) identifies the zones with the highest heat generation.

Fig. 10 Tool and workpiece information in HyperWorks

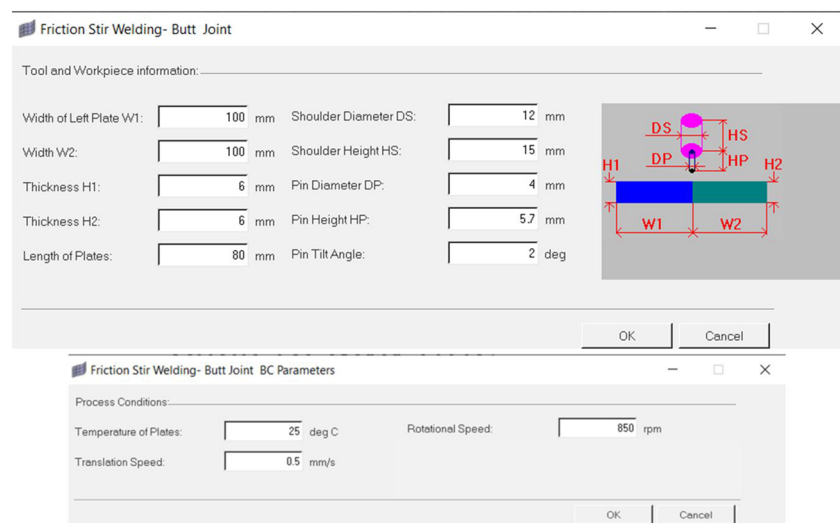


Fig. 11 Isometric view of the simulated model of the friction stir welding process showing temperature contours from minimum (blue) to maximum (red) values

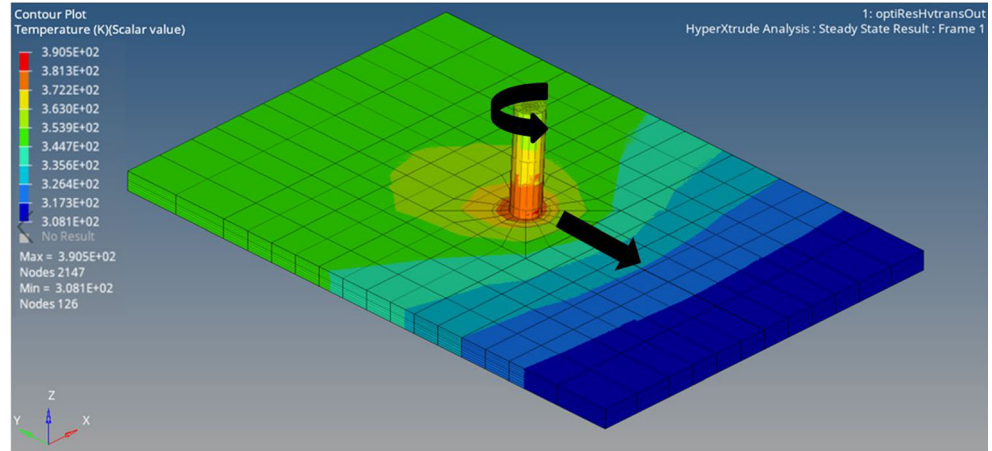


Figure 12 illustrates the temperature distribution up-view during FSW. As can be seen, the maximum generated heat is seen around the pin and shoulder, while the effect of temperature on the workpiece is degraded farther from this region.

The effect of pin penetration into the workpiece is shown in Fig. 13. Further tool penetration leads to more friction, and consequently, more heat will be generated.

The maximum heat is generated underside and around the shoulder, as well as around the pin, as was observed in experimental results. This effect was also confirmed in the numerical simulation shown in Fig. 14.

Table 7 reports the comparison between the numerical and experimental results. As can be seen from these results, the average difference is approximately 6%, which can be due to the inappropriate placement of the thermal camera. The maximum temperature difference in the numerical and experimental analysis was 15 °C, which indicates a deviation of approximately 10.5%. On the other hand, the minimum difference was about 1 °C, indicating an insignificant deviation of 0.7%.

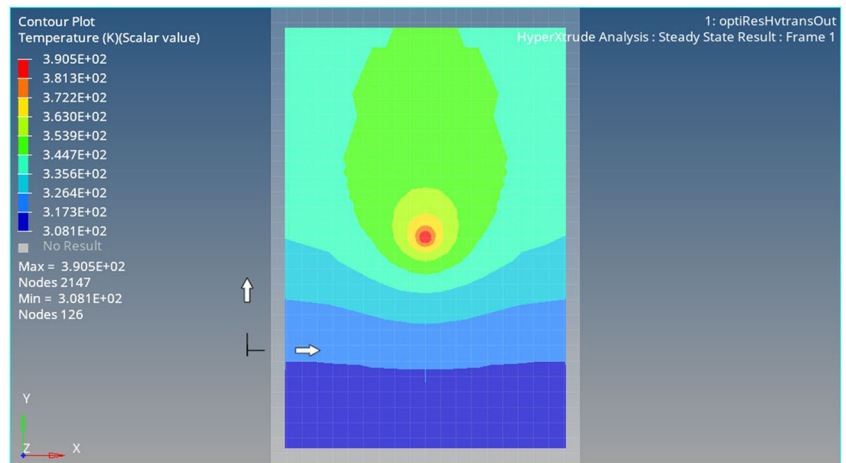
Figure 15 demonstrates the comparative plots of generated heats in numerical and experimental analysis. Although some higher and lower results were observed in numerical

simulation compared with the experimental results, the deviations were acceptable.

The effect of each processing parameter on the generated heat is illustrated in Fig. 16. According to the plots, there is a good agreement between each parameter in experimental and numerical investigations. As previously observed in the experimental model and is evident in Fig. 16a, the generated heat initially decreased slightly, followed by an increasing trend. Similar to the experimental results, the numerical simulation confirmed that the rotational speed enhancement leads to a linear response surface increment, as shown in numerical results (See Fig. 16b). Moreover, as shown in Fig. 16c, when the travel speed increased, the response surface declined. In other words, the travel speed has a deteriorating effect on the response surface, which was confirmed in both experimental and numerical analyses of the present study. As Fig. 16d shows, the experimental and numerical results are in good agreement, and the response surface inclined slightly by tool angle enhancement.

If the shoulder influences a higher area on the intersecting surface and the pin is large enough to stir on the intersect boundary (not remove the stock), then a more appropriate

Fig. 12 Temperature gradient contour in the top surface of the workpiece. During movement, the tool moves to the middle-point of the plate



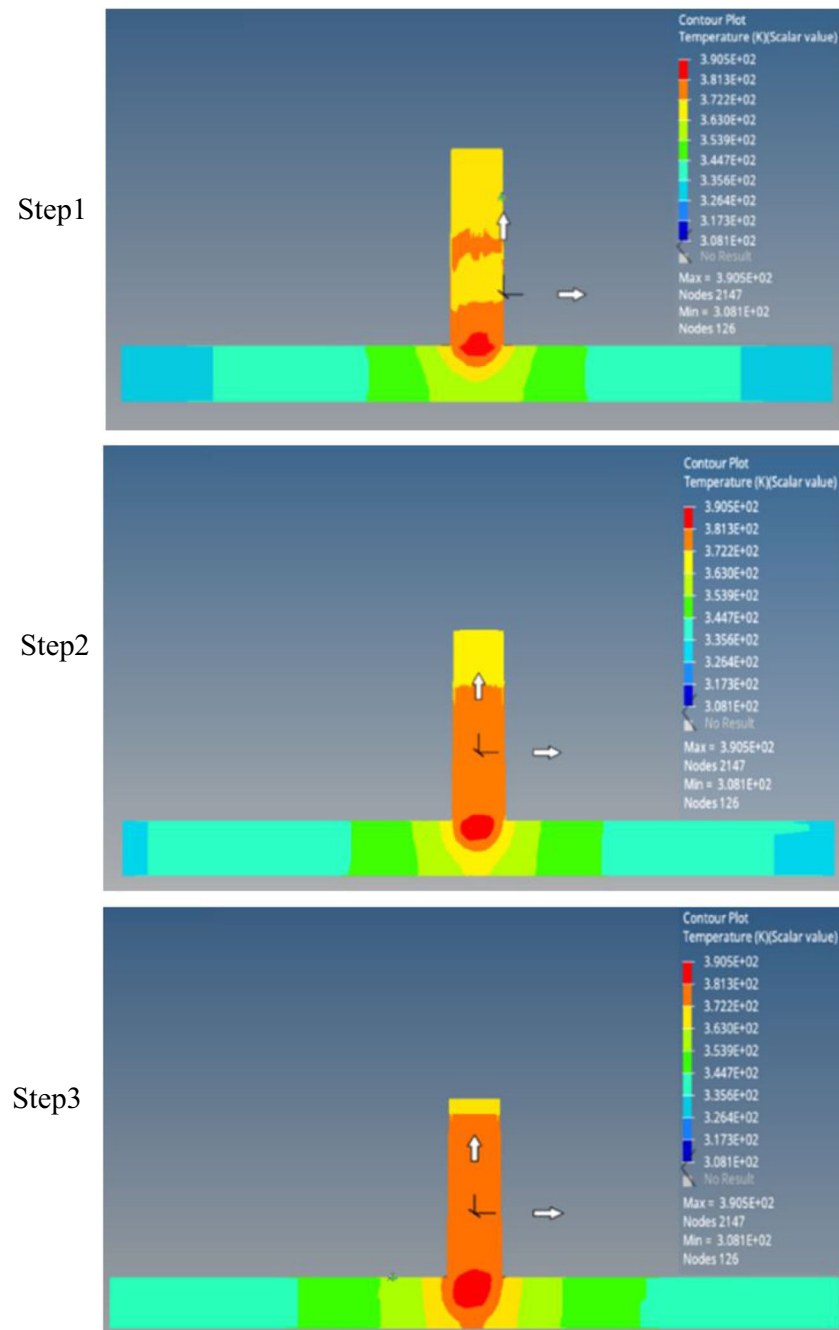


Fig. 13 Temperature history for tool and workpiece during pin penetration

joint can be obtained. As observed in the experiments and simulations of the current study, when the tool diameter ratio increased or the ratio of pin diameter to the shoulder diameter decreased, the generated heat reduced slightly and increased afterward.

Higher tilt angles applied more compressive force on the workpiece and squeezed the polypropylene sheets (similar to the forging process). Excessive tilt angles lead to stock removal from the sheet surfaces, unsettled welding uniformity, and occasional penetration of the tool into the workpiece due to

exorbitant friction and force, which result in improper connections. Proper adjustment of the tool angle improves the controllability of the generated heat to yield a proper connection. The experimental and numerical results demonstrated that the glass transition temperature is necessary to obtain an appropriate joint because the mechanical properties of the polypropylene welded using FSW are directly affected by temperature variation in the process. Therefore, it is essential to control the generated heat, especially around the glass transition temperature, to improve the welding quality.

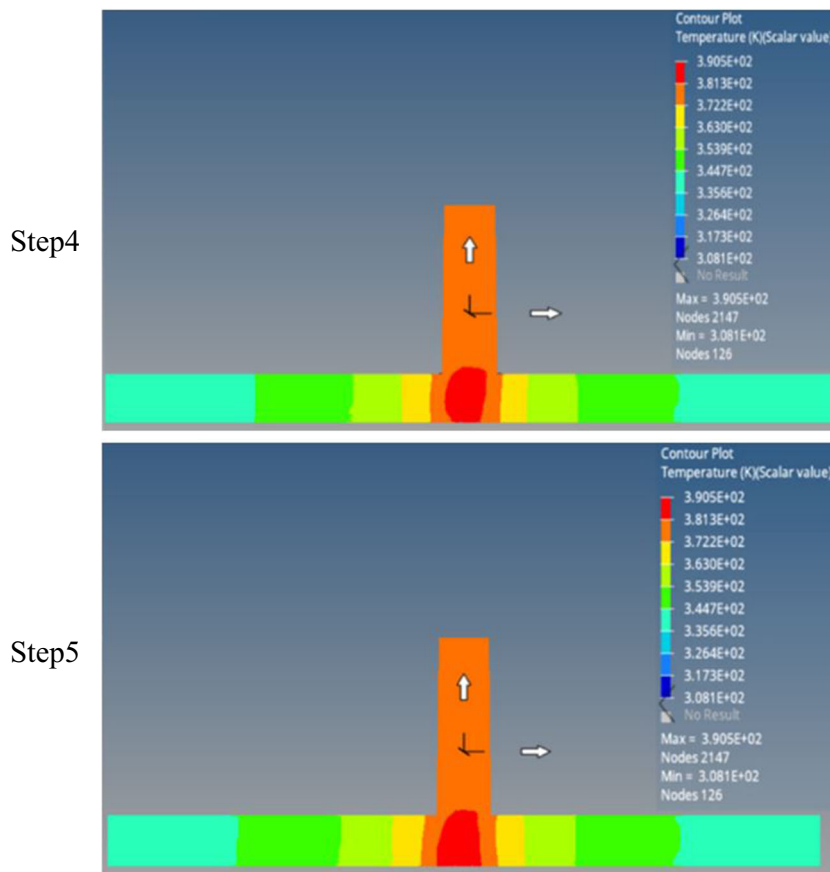


Fig. 13 (continued)

Conclusion

In this paper, the friction stir welding process for joining polypropylene sheets was investigated based on the Box-Behnken Design. To this aim, the effect of the tool’s rotational speed, travel speed, tilt angle, and diameter ratio was also studied. Moreover, the effective range of the parameters was determined based on experimental and numerical analysis. As

demonstrated in the results, proper selection of these parameters in the presented ranges controls the generated heat and consequently improves the welding quality and reduces the cost by reducing the number of required experiments.

The results show that the tool’s rotation speed (70%), diameter ratio (15%), travel speed (11%), and tilt angle (4%) affected the heat generated in the FSW process. FSW simulations using Altair’s HyperWeld provided a novel opportunity

Fig. 14 Cross-sectional view of the temperature profile

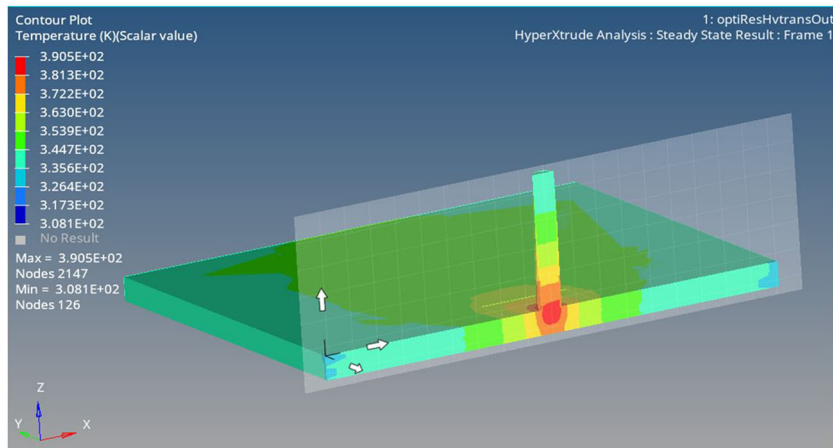


Table 7 DOE using Box-Behnken Design, and results of the comparison of the peak temperature

Run	Factor 1 A:D/d	Factor 2 B:Rotational speed	Factor 3 C:Travel speed	Factor 4 D:Title angle	Temperature (experimental) °c	Temperature (simulation) °c	Percentage difference (%)
1	3	850	30	1	158.64	146.21	-8.5
2	2	850	50	2	150.56	158.32	4.9
3	2.5	850	70	2	125.67	138.38	9.2
4	2	850	70	1	138.97	142.76	2.7
5	2.5	1000	30	1	143.65	151.61	5.3
6	2.5	850	50	1	131.66	136.80	3.8
7	3	850	50	2	144.68	140.27	-3.1
8	3	700	50	1	135.61	125.45	-8.1
9	2.5	850	50	1	132.69	136.80	3.0
10	2.5	850	30	2	146.16	145.10	-0.7
11	2.5	850	70	0	129.63	134.91	3.9
12	3	1000	50	1	149.08	146.89	-1.5
13	2	700	50	1	121.86	131.56	7.4
14	2	850	30	1	144.68	149.84	3.4
15	2.5	700	50	0	115.51	126.85	8.9
16	2	850	50	0	136.44	145.38	6.1
17	2.5	1000	70	1	127.85	142.79	10.5
18	2.5	700	30	1	119.36	129.86	8.1
19	2.5	1000	50	0	135.21	149.09	9.3
20	3	850	70	1	147.19	135.02	-9.0
21	2.5	1000	50	2	135.12	148.67	9.1
22	2	1000	50	1	148.81	156.83	5.1
23	2.5	700	50	2	118.30	128.92	8.2
24	2.5	850	30	0	123.01	132.73	7.3
25	2.5	850	50	1	135.13	136.80	1.2
26	2.5	850	50	1	132.39	136.80	3.2
27	2.5	700	70	1	114.32	121.98	6.3
28	3	850	50	0	152.05	143.01	-6.3
29	2.5	850	50	1	130.14	136.80	4.9

Fig. 15 The measured temperature along the welding line

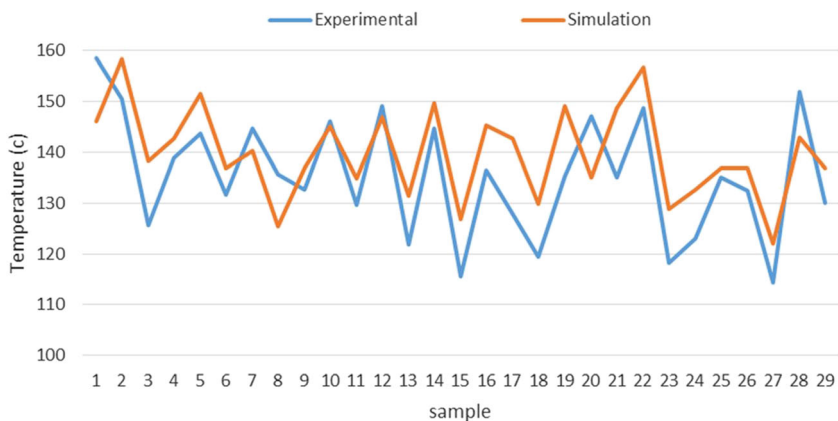
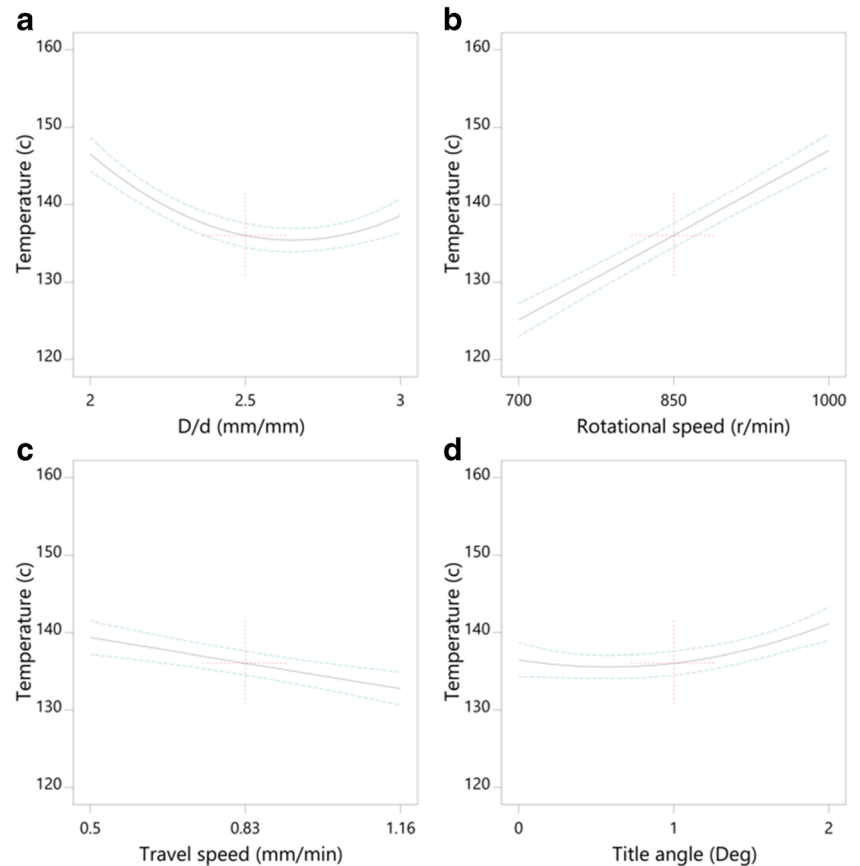


Fig. 16 The response surface diagrams plotted as a function of one parameter



to develop and extend the modeling and simulation of connection processes, which, in addition to validating practical results, provided acceptable results. The proposed model can predict the generated heat with high accuracy of 92%. The results obtained from HyperWorks software and experimental analysis indicated that there is about a 6% average difference between the experimental and numerical results, which can be due to inappropriate placement of the thermal camera. In addition, the maximum and minimum temperature difference was 15 °C (about 10.5%) and 1 °C (about 0.7%), respectively.

The increase in the rotational speed of the tool increased the generated heat due to higher friction, which improved the welding quality. However, temperature enhancement was beneficial only up to glass transition temperature. In higher temperatures, the material was deformed, and the welding quality was degraded significantly. Moreover, increasing the travel speed dissipated the generated heat and prevented the polymer sheets from reaching the glass transition temperature. On the other hand, extreme reduction in speed led to extra heat concentration on a specific area of the workpiece that deformed the sheets and decreased the welding quality. If the generated heat was maintained within the range of glass transition temperature and the melting temperature of the workpiece, the resulting fittings had higher quality. In addition, since the pin diameter reduction decreased the heat generation,

the shoulder was more responsible for the generated heat than the pin surface during the FSW process. Finally, the inlet heating (along the welding line) increased by increasing the rotational speed of the tool.

Declarations

Conflict of interest The authors declare that they have no conflict of interest.

References

- Oliveira PH, Amancio ST, Dos Santos JF et al (2010) Preliminary study on the feasibility of friction spot welding in PMMA. *J Mater Lett* 64(19):2098–2101
- Yousefpoor A, Hojjati M, Immarigeon JP (2004) Fusion bonding/welding of thermoplastic composites. *J Thermoplast Compos Mater* 17(4):303–341
- Huang Y, Meng X, Xie Y, Wan L, Lv Z, Cao J, Feng J (2018) Friction stir welding/ processing of polymers and polymer matrix composites. *Compos A: J Appl Sci Manuf* 105:235–257
- Nandan R, DebRoy T, Bhadeshia HKDH (2008) Recent advances in friction-stir welding—process, weldment structure and properties. *Prog Mater Sci* 53(6):980–1023
- Mishra RS, Ma ZY (2005) Friction stir welding and processing. *Mater Sci Eng* 50:1–78

6. Huang Y, Meng X, Xie Y, Lv Z, Wan L, Cao J, Feng J (2018) Friction spot welding of carbon fiber-reinforced polyetherimide laminate. *Compos Struct* 189:627–634
7. Amini A, Asadi P, Zolghadr P (2014) Friction stir welding applications in industry. *Advances in friction-stir welding and processing*. Woodhead Publishing Limited. Doi: <https://doi.org/10.1533/9780857094551.671>
8. Aghajani Derazkola H, Elyasi M (2018) The influence of process parameters in friction stir welding of Al-Mg alloy and polycarbonate. *J Manuf Process* 35:88–98
9. Meng X, Huang Y, Cao J et al (2021) Recent progress on control strategies for inherent issues in friction stir welding. *Prog Mater Sci* 115:1–74
10. Arici A, Selale S (2007) Effects of tool tilt angle on tensile strength and fracture locations of friction stir welding of polyethylene. *J Sci Technol Weld Join* 12(6):536–539
11. Payganeh GH, Arab NBM, Asl YD et al (2011) Effects of friction stir welding process parameters on appearance and strength of polypropylene composite welds. *Int J Phys Sci* 6:4595–4601
12. Shazly M, El-raey M (2014) Friction stir welding of polycarbonate sheets. In: Carpenter JS, Bai C, Hwang J-Y, Ikhmayies S, Li B, Monteiro SN, Peng Z, Zhang M (eds) *Characterization of minerals, metals and materials*. Wiley, Hoboken, pp 555–563
13. Threadgill PL, Leonard AJ, Shercliff HR et al (2013) Friction stir welding of aluminium alloys. *Int J Mater Rev* 54:49–93
14. Aydin M (2010) Effects of welding parameters and preheating on the friction stir welding of UHMW-polyethylene. *J Polym Plast Technol Eng* 49(6):595–601
15. Squeo E, Bruno G, Guglielmotti A, Quadrini F (2009) Friction stir welding of polyethylene sheets. *The Annals of Dunarea De Jos University of Galati, Fascicle V, Technologies in Machine Building*, ISSN: 1221-4566: 241–246
16. Panneerselvam K, Lenin K (2013) Effects and defects of the polypropylene plate for different parameters in friction stir welding process. *Int J Res Eng Technol* 2:143–152
17. Arici A, Sinmaz T (2005) Effects of double passes of the tool on friction stir welding of polyethylene. *J Mater Sci* 40(12):3313–3316
18. Roth A, Hake T, Zaeh MF (2014) An analytical approach of modeling friction stir welding. *Procedia CIRP* 18:197–202
19. Zhang Z, Zhang HW (2008) A fully coupled thermo-mechanical model of friction stir welding. *Int J Adv Manuf Technol* 37(3–4): 279–293
20. Li H, Liu D (2014) Simplified thermo-mechanical modeling of friction stir welding with a sequential FE method. *Int J Model Optim* 4(5):410–416
21. Mauricio, Pedro (2009) Modeling temperature distribution in friction stir welding using the finite element method. 20th international congress of mechanical engineering, November 15–20
22. Salloomi KN et al (2013) 3-dimensional nonlinear finite element analysis of both thermal and mechanical response of friction stir welded 2024-T3 aluminium plates. *J Inf Eng Appl* 3(9):6–15
23. Abdul Arif, et al. (2013) Finite element modelling for validation of maximum temperature in friction stir welding of aluminium alloy. 3rd international conference on production and industrial engineering, CPIE, at NIT, Jalandhar, Punjab
24. Huang Y, Xie Y, Meng X, Lv Z, Cao J (2018) Numerical design of high depth-to-width ratio friction stir welding. *J Mater Process Technol* 252:233–241
25. Armansyah et al (2014) Temperature distribution in friction stir welding using finite element method. *World Acad Sci, Eng Technol, Int J Mech, Aerosp, Ind Mechatronics Eng* 8(10):1699–1704
26. Kiral BG et al (2013) Finite element modeling of friction stir welding in aluminum alloys joint. *Math Comput Appl* 18(2):122–131
27. Zhang Z, Zhang HW (2009) Numerical studies on the effect of transverse speed in friction stir welding. *Mater Des* 30(3):900–907
28. Prasanna P et al (2010) Finite element modeling for maximum temperature in friction stir welding and its validation. *Int J Adv Manuf Technol* 51(9–12):925–933
29. Hasanzadeh R, Azdast T, Doniavia A, Lee RE (2019) Multi-objective optimization of heat transfer mechanisms of microcellular polymeric foams from thermal-insulation point of view. *Therm Sci Eng Prog* 9:21–29
30. Azdast T, Hasanzadeh R, Moradian M (2017) Optimization of process parameters in FSW of polymeric nanocomposites to improve impact strength using step wise tool selection. *Mater Manuf Process* 33(3):343–349
31. Mosavvar A, Azdast T, Moradian M, Hasanzadeh R (2019) Tensile properties of friction stir welding of thermoplastic pipes based on a novel designed mechanism. *Weld World* 63(3):691–699
32. Azdast T, Hasanzadeh R (2019) Experimental assessment and optimization of shrinkage behavior of injection molded polycarbonate parts. *Mater Res Express* 6(11):115334
33. Hasanzadeh R, Azdast T, Doniavi A, Rostami M (2019) A prediction model using response surface methodology based on cell size and foam density to predict thermal conductivity of polystyrene foams. *Heat Mass Transf* 55(10):2845–2855
34. Mendes N, Loureiro A, Martins C, Neto P, Pires JN (2014) Morphology and strength of acrylonitrile butadiene styrene welds performed by robotic friction stir welding. *J Mater Des* 64:81–90
35. Azarsa E, Mostafapour A (2014) Experimental investigation on flexural behavior of friction stir welded high density polyethylene sheets. *J Manuf Process* 16(1):149–155
36. Rahbarpour R, Azdast T, Rahbarpour H, Shishavan SM (2014) Feasibility study of friction stir welding of wood-plastic composites. *J Sci Technol Weld Join* 19(8):673–681
37. Mostafapour A, Asad FT (2016) Investigations on joining of nylon 6 plates via novel method of heat assisted friction stir welding to find the optimum process parameters. *J Sci Technol Weld Join* 21(8):660–669
38. Bagheri A, Azdast T, Doniavi A (2013) An experimental study on mechanical properties of friction stir welded ABS sheets. *J Mater Des* 43:402–409
39. Sajed M, Bisadi H (2016) Experimental failure study of friction stir spot welded similar and dissimilar aluminum alloys. *J Weld World* 60(1):33–40
40. Badarinarayan H, Shi Y, Li X, Okamoto K (2009) Effect of tool geometry on hook formation and static strength of friction stir spot welded aluminum 5754-O sheets. *Int J Mach Tools Manuf* 49(11): 814–823
41. Box GEP, Behnken DW (1960) Some new three level designs for the study of quantitative variables. *J Technometrics* 2(4):455–475
42. Ferreira SLC, Bruns RE, Ferreira HS, Matos GD, David JM, Brandão GC, da Silva EGP, Portugal LA, dos Reis PS, Souza AS, dos Santos WNL (2007) Box-Behnken design: an alternative for the optimization of analytical methods. *J Anal Chim Acta* 597(2):179–186
43. Kamarei F, Ebrahimzadeh H, Yamini Y (2010) Optimization of solvent bar micro extraction combined with gas chromatography for the analysis of aliphatic amines in water samples. *J Hazard Mater* 178(1–3):747–752
44. Karthikeyan R, Balasubramanian V (2010) Predictions of the optimized friction stir spot welding process parameters for joining AA2024 aluminum alloy using RSM. *Int J Adv Manuf Technol* 51(1–4):173–1830
45. Khuri AL, Cornell J (1996) *Response surfaces: design and analysis*, 2nd edn. Marcel Dekker, New York
46. Khandkar MZH, Khan JA, Reynolds AP (2003) Prediction of temperature distribution and thermal history during friction stir

- welding: input torque based model. *Sci Technol Weld Join* 8(3): 165–174
47. Woo W, Balogh L, Ungár T, Choo H, Feng Z (2008) Grain structure and dislocation density measurements in a friction-stir welded aluminum alloy using X-ray peak profile analysis. *Mater Sci Eng A* 498(1–2):308–313
 48. Nandan R, Roy G, Lienert T, Debroy T (2007) Three-dimensional heat and material flow during friction stir welding of mild steel. *Acta Mater* 55(3):883–895
 49. Ansari MA, Samanta A, Behnagh RA, Ding H (2019) An efficient coupled Eulerian-Lagrangian finite element model for friction stir processing. *Int J Manuf Technol* 101(5–8):1495–1508
 50. Eskandari M, Aval HJ, Jamaati R (2019) The study of thermomechanical and microstructural issues in dissimilar FSW of AA6061 wrought and A390 cast alloys. *J Manuf Process* 4: 168–176

Publisher's note Springer Nature remains neutral with regard to jurisdictional claims in published maps and institutional affiliations.